Available online at www.sciencedirect.com
SCIENCE DIRECT®
International Journal of Thermal Sciences 44 (2005) 399–409
International Journal of Thermal Sciences
www.elsevier.com/locate/ijts

Radiation heat transfer in circulating fluidized bed combustors

Morgan Eriksson [a], Mohammad R. Golriz [a,b,*]

[a] *Department of Applied Physics and Electronics, Umeå University, SE-901 87 Umeå, Sweden*
[b] *Department of Mechanical and Aerospace Engineering, Carleton University, 1125 Colonel By Drive, Ottawa, ON K1S 5B6, Canada*

Received 18 November 2003; received in revised form 21 October 2004; accepted 2 November 2004

Abstract

A new model for predicting radiation heat transfer in circulating fluidized bed combustors is proposed. The model assumes two phase structure, the flow at the wall dominated by streamers of clusters traveling mostly downward, interspersed with periods where there is upwards flow of a dilute suspension. Also, the model assumes the intensity distribution to be semi-isotropic in the forward and backward direction. The predictions are in good agreement with the experimental results from the literature. Finally, a parametric study is performed to show the effect of different bed parameters on radiative heat transfer. The results indicate that suspension temperature, wall temperature, wall emissivity, particle emissivity, and suspension density have significant influence on the radiation heat transfer coefficient.

Keywords: Fluidization; Heat transfer; Radiation; Circulating fluidized bed; Combustion; Modeling

1. Introduction

Circulating Fluidized Bed (CFB) combustion technology has grown in importance during the last two decades as boiler manufacturers have recognized the advantages of this technology, such as outstanding fuel flexibility, low emission of pollutants and adaptability to load change. Today hundreds of CFB boilers are in use or under construction worldwide. Developing a good understanding of heat transfer in fluidized beds is essential for proper design and optimization of these boilers. Several different operating parameters influence combustion and heat transfer processes. Flow patterns in a CFB riser are divided into two major sections: a dilute core region where particles are transported upwards by flowing gases, and a denser wall layer region where particles reverse their flow directions and descend along the wall, see [1–8] among others. This descending wall layer contributes a majority of the heat transfer gained from conduction/convection, but also forms a shielding curtain that decreases the contribution from radiation [9–11]. The parameters described in the following have been found to be the most important ones for the heat transfer processes.

Bed particle size. When radiation heat transfer is considered, particle size has an influence on the suspension absorption and scattering coefficients whose sizes are proportional to $1/d_p$ [12]. Finer particles (for the same voidage) function as a denser curtain between the high temperature core and the colder wall, thus decreasing the net radiation flux. Where radiation is not significant, it can be expected that the total heat flux will increase with decreasing particle size, mainly due to shorter average distances for conduction between the wall and adjacent particles [1,13–15]. But at high suspension temperatures, the situation is more complex since the particle diameter affects the convection/conduction and radiation heat transfer in opposite directions.

Suspension density. Suspension density is generally recognized as a dominant factor influencing CFB heat transfer, and many researchers have related their experimental heat transfer data to the cross-sectional average suspension den-

* Corresponding author. Phone: +1 613 520 2600 ext. 8581, fax: +1 613 520 5715.
E-mail addresses: mgolriz@mae.carleton.ca, mohammad.golriz@tfe.umu.se (M.R. Golriz).

1290-0729/$ – see front matter © 2005 Elsevier SAS. All rights reserved.
doi:10.1016/j.ijthermalsci.2004.11.006

Nomenclature

a	absorption coefficient for gray medium	m^{-1}
a_λ	absorption coefficient at wavelength λ	m^{-1}
A	area	m^2
B	back-scatter fraction	
c	volumetric particle concentration	
c_{cl}	average volumetric particle concentration in clusters	
d_p	particle diameter	m
D_R	riser diameter	m
e	emissivity	
e_b	bulk emissivity	
e_p	particle emissivity	
e_w	wall emissivity	
f	fraction of wall covered by clusters	
F	view-factor	
g	gravitational acceleration	$m{\cdot}s^{-2}$
h	total heat transfer coefficient	$W{\cdot}m^{-2}{\cdot}K^{-1}$
h_r	radiation heat transfer coefficient	$W{\cdot}m^{-2}{\cdot}K^{-1}$
H	height of riser	m
i'_λ	spectral radiation intensity	$W{\cdot}m^{-2}{\cdot}\mu m^{-1}{\cdot}sr^{-1}$
$i'_{\lambda b}$	spectral radiation intensity from black body	$W{\cdot}m^{-2}{\cdot}\mu m^{-1}{\cdot}sr^{-1}$
I^+	radioactive heat flux in positive direction	$W{\cdot}m^{-2}$
I^-	radioactive heat flux in negative direction	$W{\cdot}m^{-2}$
I_b	emissive power of black body	$W{\cdot}m^{-2}$
K	proportionality factor	
P	pressure Pa	
q_{cl}	net radiation heat flux for cluster covered section of wall	$W{\cdot}m^{-2}$
q_{di}	net radiation heat flux for section of wall covered by dilute suspension	$W{\cdot}m^{-2}$
q''_r	net radiation heat flux	$W{\cdot}m^{-2}$
R	thermal resistance	$m^2{\cdot}K{\cdot}W^{-1}$
Re_p	particle Reynolds number, $U_g d_p/\nu_g$	
s	scattering coefficient of gray medium	m^{-1}
s_λ	scattering coefficient at wavelength λ	m^{-1}
T	temperature	K
T_b	bulk temperature	K
T_{gg}	horizontal gas temperature gradient	$K{\cdot}m^{-1}$
T_w	wall temperature	K
U_g	gas velocity	$m{\cdot}s^{-1}$
x	horizontal coordinate, directed from wall towards center of riser	m
X	half the hydraulic diameter of riser	m
z	vertical coordinate, directed upwards	m

Greek letters

δ	wall layer thickness	m
ε	suspension voidage	
ε_{mf}	suspension voidage at minimum fluidization	
ε_{cs}	cross-sectional average suspension voidage	
λ	radiation wavelength	μm
ν_g	kinematic viscosity of combustion gases	$m^2{\cdot}s^{-1}$
ρ_g	combustion gas density	$kg{\cdot}m^{-3}$
ρ_p	particle density	$kg{\cdot}m^{-3}$
ρ_{sus}	suspension density	$kg{\cdot}m^{-3}$
σ	Stefan–Boltzmann constant, $= 5.67e{-}8$	$W{\cdot}m^{-2}{\cdot}K^{-4}$
ϕ	dimensionless distance in riser, $1 - x/X$	
Φ	scattering phase function	
Φ_s	particle sphericity	
ω	solid angle	sr

sity, see, i.e., [11,16–20]. Particle concentration in the annulus wall layer increases if suspension density increases [21]. Increased wall coverage is also a side-effect from increasing riser diameter, D, since the perimeter per unit cross-sectional area decreases and there is less wall surface available for down-flow of particles [22]. The thickness of the annular wall layer also increases, though not in proportion to the column diameter. The thickness is approximately proportional to $D^{0.57}$ according to a correlation given by Werther [23]. A thicker wall layer and higher particle concentration increases the radiation resistance between core and wall, thereby decreasing the radiation contribution.

Superficial gas velocity. Increased superficial gas velocity can cause more particles to be carried out at the top of the riser, leading to decreasing pressure drop per unit length of the riser for the same solids circulation rate [24]. Thus with a constant solids circulating rate and increasing superficial gas velocity, the suspension density will decrease, resulting in a thinner wall layer and thus in increasing radiation heat transfer coefficients. If the superficial gas velocity is increased while adjusting the solids circulation rate to maintain constant suspension density, heat transfer coefficients will not change significantly [1]. However, increased gas velocities with constant suspension densities might cause the density profile to change, thereby indirectly affecting heat transfer coefficients. The superficial gas velocity effect on heat transfer coefficients mainly depends on its effect on solids motion near the wall [6].

Cluster formations. It is generally agreed that in a fast fluidized bed, the suspension partly condenses into denser clusters that move upwards through the core of the riser [3, 9,25–27]. At some point, they get swept towards the low velocity region near the wall, where clusters reverse their flow direction and start falling along the wall. The clusters do not

usually remain attached close to the wall through the entire height of the riser. After falling 1–3 m [28,29], they either lose their identity due to shear force of the gas or the impact of other particles, and they may also simply detach themselves from the wall and enter the core region again. Dense clusters functions as a thicker radiation shield, and a high fraction of wall coverage by clusters can therefore decrease the radiation flux.

Gas gap thickness. Falling particles and clusters are separated from the riser wall by a thin gas film of order the mean particle diameter [25,26,30–32]. Significant effect from this gas gap thickness has been seen on the conduction term in heat transfer, as a larger gap thickness causes larger thermal resistance, but little influence has been seen on the radiation term [33]. This is obvious since the view factor between wall and bed will approach unity regardless of variations of this limited distance, and the small amount of particle-free gas can be considered as fully transparent. The effect of this factor is therefore neglected in this work.

Membrane wall geometry. The membrane walls of a CFB riser that surrounds the fluidized bed are made up of vertically directed tubes, which are welded to lateral fins separating two adjacent tubes. Each fin, sided by tubes, forms a cavity that affects the solids flow. As a cluster reaches the wall, it mainly get trapped in the fin cavity region where it falls in structures similar to waves of strands or streamers [6, 9]. Particles which are concentrated over the fins stay there longer than those traveling on the crest of the tubes, and the combination of longer residence time and lower view factor from the fin towards the hot core region lead to smaller heat transfer coefficients on the fins. It can be as low as half of that on the tube crest [9,16,34].

Bulk temperature. Heat transfer coefficients increase with increasing bulk temperature, and this fact has been attributed to the increase in thermal conductivity of the fluidizing gas and to an increase in radiation at higher temperatures. At low temperatures the radiation component is negligible, but above 500 °C heat transfer coefficients increase predominantly because of the fast growing T^4-factor of the radiation component [5,35]. Radiation is therefore an important mode of heat transfer in industrial CFB boilers, where temperatures usually ranges from 800 to 900 °C, and typically makes up for about 25 to 50% of the total heat transfer coefficient [36].

2. Modeling of radiation heat transfer

The thermal resistance for radiation heat transfer between two surfaces (i and j) is given by

$$R_{i-j} = \frac{1-e_i}{A_i e_i} + \frac{1}{A_i F_{i-j}} + \frac{1-e_j}{A_j e_j} \tag{1}$$

where e denotes emissivity and F is a view factor. The net radiation heat transfer between the two surfaces is then given by

$$q_r'' = \frac{\sigma(T_i^4 - T_j^4)}{R_{i-j}} \tag{2}$$

The radiation heat transfer coefficient is defined as

$$h_r = \frac{q_r''}{T_i - T_j} \tag{3}$$

If the bed core and riser wall are considered as two infinite parallel plates with view factor 1, we can express the thermal resistance per unit area, as

$$R_{b-w} = \frac{1}{e_b} + \frac{1}{e_w} - 1 \tag{4}$$

By substituting Eqs. (2) and (4) into Eq. (3), we can calculate the maximum possible radiation heat transfer coefficient for this case from

$$h_{r,\max} = \frac{\sigma(T_b^2 + T_w^2)(T_b + T_w)}{\frac{1}{e_b} + \frac{1}{e_w} - 1} \tag{5}$$

This is the maximum radiative heat transfer coefficient, $h_{r,\max}$, which could theoretically occur in CFBs, and it can be used as a upper limit for real values in a CFB boiler, where influences by dampening factors be considered.

2.1. Radiation heat transfer in participating media

Absorption and emission are the dominant mechanisms of radiation heat transfer through homogeneous media such as gases. An additional mechanism of scattering (reflection, refraction and diffraction) is introduced if the media contains inhomogeneities, such as particles in CFBs. Radiation heat transfer processes within a CFB usually originates as emissions from the gas-solid suspension in the core and from the riser walls. This radiation undergoes complex interactions with the suspension, primarily due to absorption, emission and scattering processes. Three dominant factors have been used to characterize radiation interactions within the suspension: the *absorption coefficient* (a), the *scattering coefficient* (s) and the *scattering phase function* (Φ). The propagation of radiation within absorbing, emitting and scattering media is governed [37,38] by

$$\frac{\mathrm{d}i'_\lambda}{\mathrm{d}T_{gg}} = -a_\lambda i'_\lambda(T_{gg}) - s_\lambda i'_\lambda(T_{gg}) + a_\lambda i'_{\lambda b}(T_{gg}) + \frac{s_\lambda}{4\pi} \int_{\omega_i=0}^{4\pi} i'_\lambda(T_{gg}) \Phi(\lambda, \omega, \omega_i)\, \mathrm{d}\omega_i \tag{6}$$

The first two terms on the right side represents decreasing radiation due to absorption and scattering, respectively. The third term gives the flux due to emission. The last term represents gain from scattering into the direction under consideration from all other directions. The radiative intensity, i'_λ,

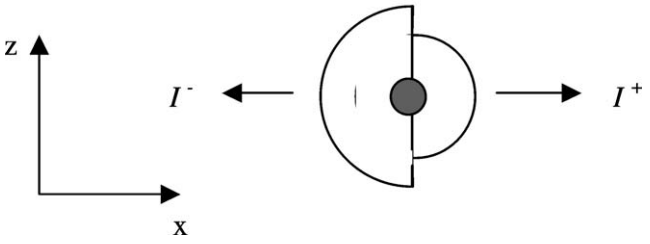

Fig. 1. The two-flux model by one particle, having symmetric radiation flux but of different strength in positive and negative directions.

is defined as the energy per unit area per unit solid angle per unit wavelength. Note that the scattering phase function $\Phi(\lambda, \omega, \omega_i) = 1$ for isotropic scattering (symmetric in all directions). The absorption and scattering coefficients are defined as the fraction of the corresponding energy loss from the propagating wave per unit length of travel.

When particles are present or are injected into a gas to enhance its absorption or emission of radiation, the gas-particle mixture may act as nearly gray [37]. For gray media, the absorptivity is equal to the emissivity, and there is no wavelength dependency. Eq. (6) may therefore be written

$$\frac{\mathrm{d}i'}{\mathrm{d}T_{gg}} = -ai'(T_{gg}) - si'(T_{gg}) + ai'_b(T_{gg}) + \frac{s}{4\pi}\int_{\omega_i=0}^{4\pi} i'(T_{gg})\Phi(\omega, \omega_i)\,\mathrm{d}\omega_i \tag{7}$$

If net radiation heat transfer is developed in only one dimension, the transfer equation can be reduced to the expression from the *two-flux model* [12,39,40], which describes the differential variations in the intensities of forward and backward radiation fluxes along this one-dimensional transport direction, see Fig. 1. Emission and scattering from particles are assumed to be symmetric but having different strengths in positive (forward) and negative (backward) directions.

Brewster and Tien [12] studied cases where the particles were large enough that

$$\frac{\pi d_p}{\lambda} > 5 \tag{8}$$

The assumption of independent scattering is then made, where each particle acts as a point scatterer. This means that interactions of the particles with the radiation field are not influenced by the presence of neighboring particles. This condition is respected when the distance between neighboring particles, on the average, is large enough in comparison to their diameters and to the radiation wavelength. If particles are assumed to be opaque gray spheres, and independent and semi-isotropic scattering is present, the simplified two-flux equations for radiation heat flux can be written

$$\frac{\mathrm{d}I^+}{\mathrm{d}x} = -(a + sB)I^+ + sBI^- + aI_b(x) \tag{9}$$

$$\frac{\mathrm{d}I^-}{\mathrm{d}x} = -(a + sB)I^- + sBI^+ + aI_b(x) \tag{10}$$

where B is the back-scatter fraction

$$a = K\frac{3ce_p}{\mathrm{d}_p} \tag{11}$$

$$s = K\frac{3c(1-e_p)}{\mathrm{d}_p} \tag{12}$$

where K is a proportionality factor.

Consider the right side of Eq. (9). The first negative terms represents a decrease in radiation flux towards the positive direction due to absorption and due to back-scattering towards the negative direction, in this slice of the suspension layer. This is a shielding effect from the particulate media, sometimes accounted for as a combined *extinction coefficient.* Continuation of positive flux is represented by back-scatter from flux that was going in the negative direction, and from the last emission term, given according to the Stefan–Boltzmann law by

$$I_b(x) = \sigma T^4/\pi \tag{13}$$

I_b is a function of x since the temperature level is dependent on x-position. In the last term of Eq. (9), a represents an effective emissivity of the suspension layer, since we have assumed gray media and absorptivity equals emissivity.

Brewster and Tien [12] gave no value for the proportionality factor K of Eqs. (11) and (12), but assumed it to be a constant that would have to be determined experimentally. Chen et al. [40] concluded that this factor adjusts the optical thickness of the gas-particle mixture with a larger K corresponding to an optically thicker suspension. Consider an average volumetric particle concentration, $c = 0.01$ in the transport section of a CFB riser, particle emissivity, $e_p = 0.6$ and particle diameter $d_p = 260$ μm. By assuming $K = 1$, the extinction coefficient will be 100 which indicates any radiation flux trying to penetrate even in this relatively dilute suspension would be entirely extinguished within a depth of $1/100 = 0.01$ m. This could hardly be the case and therefore $K \ll 1$ as Chen et al. [40] experimented with K-values in the range of 10^{-3} to 1.

2.2. The model

The model in this work is based on the two-flux method for calculating radiation heat transfer in particulate media. Many researchers have begun with a two-phase structure, with the flow at the wall dominated by streamers of clusters traveling mostly downward, interspersed with periods where there is upwards flow of a dilute suspension, see Fig. 2.

Previous models, such as the *continuous emulsion model* and the *non-uniform emulsion model*, have been solved mathematically using advanced finite element method or discrete ordinate method, see, i.e., Flamant et al. [36] and Luan et al. [42]. To be able to use the model and predict h_r, some parameters such as temperature profile, horizontal variations of density, properties of cluster, fraction of wall which is covered by clusters, and wall layer thickness have to be

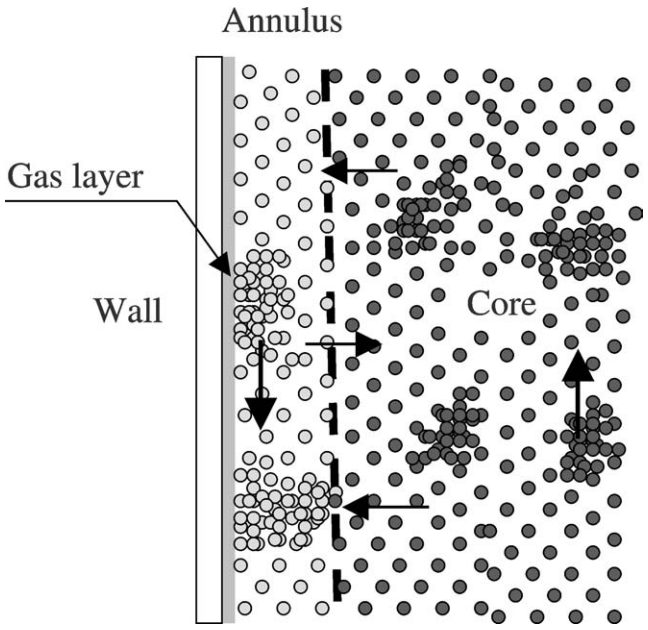

Fig. 2. Conceptual view of cluster of particles and gas close to a wall.

estimated. The following estimations were made for the proposed model:

Temperature gradient within the bed is obtained by employing the correlation proposed by Golriz [32], i.e.,

$$\frac{T-T_w}{T_b-T_w} = 1-\left[-0.023Re_p+0.094(T_b/T_w)+0.294(z/H)\right] \times \exp\left[-0.0054(x/d_p)\right] \quad (14)$$

where $Re_p = U_g d_p/\nu_g$. As noted above, the descending wall layer is often divided into two different sections, one where the wall is covered by clusters descending along the wall, and the other where the very dilute suspension of the inner core region extends all the way to the wall. We use the correlation proposed by Issangya et al. [43] to describe the radial variation of voidage, i.e.,

$$\varepsilon(\phi) = \varepsilon_{\mathrm{mf}} + (\varepsilon_{\mathrm{cs}}-\varepsilon_{\mathrm{mf}})\varepsilon_{\mathrm{cs}}^{(-1.5+2.1\phi^{3.1}+5.0\phi^{8.8})} \quad (15)$$

where $\phi = 1-x/X$. Average voidage for the dilute portion of the wall layer is assumed to be the value of ε at $x = X/3$. Note that Eq. (15) and some other equations below are for circular cross-section. The volumetric particle concentration at this location is then

$$c = 1-\varepsilon(\phi) \quad (16)$$

The voidage at minimum fluidization is estimated from the correlation by Shafey et al. [44]:

$$\varepsilon_{\mathrm{mf}} = (14\Phi_s)^{-1/3} \quad (17)$$

where Φ_s is the sphericity of the bed particles. For perfect spheres $\Phi_s = 1$. In this study, bed particles are assumed to be slightly less than perfect spheres, with $\varepsilon_{\mathrm{mf}} = 0.42$.

$\varepsilon_{\mathrm{cs}}$ represents the cross-sectional average voidage. In CFB boilers, there are usually several measurement points for reading pressure-drops along the height of the riser. If the influences of acceleration and wall friction on the pressure-drop term are neglected compared to the pressure-drop from supporting the suspension,

$$\Delta P = \rho_{\mathrm{sus}} g \Delta z \quad (18)$$

where

$$\rho_{\mathrm{sus}} = \rho_p(1-\varepsilon_{\mathrm{cs}}) + \rho_g \varepsilon_{\mathrm{cs}} \quad (19)$$

and thus

$$\varepsilon_{\mathrm{cs}} = \frac{\rho_p - \rho_{\mathrm{sus}}}{\rho_p - \rho_g} \quad (20)$$

since $\rho_p \gg \rho_g$, we can take

$$\varepsilon_{\mathrm{cs}} = 1 - \frac{\rho_{\mathrm{sus}}}{\rho_p} \quad (21)$$

For the wall portion covered by clusters, the average volumetric particle concentration of the clusters is obtained from the correlation by Lints [45],

$$c_{\mathrm{cl}} = 1.23c^{0.54} \quad (22)$$

The fraction of the wall covered by clusters (f) is estimated from the correlation of Lints and Glicksman [25],

$$f = 3.5c^{0.37} \quad (23)$$

The correlation of Bi et al. [21] is used to estimate the wall layer thickness, i.e.,

$$\delta = X\left(1-\sqrt{1.34-1.30(1-\varepsilon_{\mathrm{cs}})^{0.2}+(1-\varepsilon_{\mathrm{cs}})^{1.4}}\right) \quad \text{for } 0.80 \leqslant \varepsilon_{\mathrm{cs}} \leqslant 0.9985 \quad (24)$$

If the temperature boundary layer continues beyond this thickness, Eq. (15) is used to obtain voidage values.

Two separate radiation flux calculations are made; one for the wall section covered by clusters, q_{cl}, and one for the section not covered, q_{di}. The two results are then weighted together as

$$q_r'' = f q_{\mathrm{cl}} + (1-f) q_{\mathrm{di}} \quad (25)$$

The radiation heat flux calculation is started in the positive x-direction by a wall boundary condition,

$$I^+ = e_w \sigma T_w^4 + (1-e_w) I^- \quad (26)$$

where the first term on the right side represents emission from the wall, and the second term represents reflection from the radiation flux in the negative direction.

At first, no I^- values are known. Therefore, all negative direction fluxes are preset to zero. Discrete Δx-steps are then made, with an average temperature for the step obtained from Eq. (14), and an average volumetric particle concentration from Eqs. (15) or (22). To calculate the increase or decrease in positive direction radiation flux, we use

$$\Delta I^+ = \Delta x\left(-(a+sB)I^+ + sBI^- + a\sigma T^4\right) \quad (27)$$

The back-scatter fraction $B = 0.667$ for diffusely reflecting particles [12] has been generally accepted as a realistic assumption for CFB particles and is therefore adopted to this work.

The first two Δx-steps used have length 10 μm, then a Fibonacci sequence

$$\text{step}_{n+2} = \text{step}_n + \text{step}_{n+1} \quad (n = 1, 2, 3, \ldots) \tag{28}$$

is used to gradually increase the step-length as the temperature gradient becomes less steep, up to a maximum of 1 mm. These steps continue until the edge of the temperature boundary layer defined as $(T - T_w)/(T_b - T_w) = 0.995$. Here a bulk boundary condition is set as

$$I^- = e_b \sigma T_b^4 + (1 - e_b) I^+ \tag{29}$$

and the flux equation for negative direction

$$\Delta I^- = (-)\Delta x\left(-(a + sB)I^- + sBI^+ + a\sigma T^4\right) \tag{30}$$

is used to start calculation steps back towards the wall again. The first $(-)$ sign on the right side indicates that we now use steps in the negative direction, but in calculations positive step-values are still used. Now we have I^- from the preceding step and I^+ from the next step ahead, making full calculations for each step possible. But since I^- was taken as zero during the first round, we make several iterations back and forth through the temperature boundary layer, until the levels converge and we get less than a 0.01% change in the net heat flux received by the wall. The thermal boundary layer thickness is defined as the distance from the wall surface where the dimensionless temperature, $(T - T_w)/(T_b - T_w)$, is 0.995. The details of this process were explored by Eriksson [41].

Emissivity values for real surfaces are not always easy to determine, especially for a high temperature environment such as in a CFB combustor. Emissivity also varies with surface smoothness, typically being smaller for a highly polished surface than for a rough one, and it usually varies with temperature as well. Particle emissivity, $e_p = 0.6$ and wall emissivity, $e_w = 0.8$ are used in this work.

Different correlations for effective bulk emissivity have been proposed. Typically they refer to particle emissivity and sometimes also to combustion gas emissivity. Values for total bulk emissivity given by different correlations ranges from about 0.8 to 1. A correlation adopted to this study for obtaining effective bulk emissivity of a particulate media like the one found in a CFB suspension, which give $e_b \approx 0.84$ for $e_p = 0.6$, has been derived by Brewster [39] using the two-flux method and referring to particle emissivity and back-scatter fraction, as

$$e_b = \left[\frac{e_p}{(1 - e_p)B}\left(\frac{e_p}{(1 - e_p)B} + 2\right)\right]^{1/2} - \frac{e_p}{(1 - e_p)B} \tag{31}$$

3. Results and discussion

In order to compare the simulation predictions with the experimental results available in the literature, there are cases where values of some parameters are not specified. In such cases the values listed in Table 1 have been used unless noted otherwise. The proportionality factor, $K = 1/20\,000$ has been used based on experimenting with the behavior of the model [41]. In simulations of small laboratory units the thermal boundary layer, $(T - T_w)/(T_b - T_w) = 0.995$ was terminated at the half-way level. This was since the Eq. (14) is a correlation based on experimental temperature measurements at membrane wall in industrial CFB boilers.

Table 1
Parameter values used for the simulation

Parameter	
Bulk temperature, T_b	850 °C
Wall temperature, T_w	210 °C
Wall emissivity, e_w	0.8
Particle emissivity, e_p	0.6
Particle diameter, d_p	260 μm
Particle density, ρ_p	2600 kg·m^{-3}
Cross-sectional average bed density	30 kg·m^{-3}
Riser cross-section length	3 m
Riser cross-section width	3 m
Dimensionless height above the distributor (z/H)	0.5
Superficial gas velocity, u	5 m·s^{-1}

3.1. Comparisons between calculations and experiments

The total heat transfer coefficient between circulating fluidized bed and heat exchange surfaces in both large scale as well as laboratory scale risers have been measured and reported in numerous papers [1,4,10,17–19,45–47] among others. Unfortunately, much of data were limited to small scale and low temperature conditions. However, the contribution of radiation to the overall heat transfer process in the operating temperature range of 600–900 °C is still in question. Most of investigators have reported indirect radiative heat transfer coefficient see Steward et al. [7], Werdermann and Werter [10], Golriz and Sunden [31], and Wu et al. [35] among others. Predictions from the present model fall relatively close to the h_r estimated by authors from total heat flux measurements for large-scale CFB boilers, as well as Wu et al. [35] for a laboratory scale CFB, as shown in Table 2. There are only a few investigators that measured direct radiative heat flux with a probe, i.e., Luan et al. [42], Basu and Konuche [48], and Han and Cho [49]. In this work, we compare the results of the prediction with the experimental data of those works that measured direct radiative heat transfer coefficient. The dimensions and operating conditions on these units are summarized in Table 3.

Basu and Konuche [48] measured local radiative heat transfer coefficient in a 6.7 m high, 0.20 m × 0.20 m cross-sectional area riser by means of a window probe. The probe consisted of two 38.1 mm diameter quartz glass placed 3 mm apart in front of the receiving brass cylinder. The body of the probe was made of a 14 mm long and 25.4 mm diameter stainless steel plug, one end of which was heated by the bed while the other end was cooled by water. Tests were carried

Table 2
Operating conditions and comparison of model prediction with the estimated h_r from high temperature experimental data

Author	Steward et al. [7]	Werdermann and Werther [10]	Golriz and Sunden [31]	Wu et al. [35]
Bulk temperature [°C]	850	858	800–850	701
Probe surface or wall temperature [°C]	279	340	210	83
Probe surface or wall emissivity	0.85	N/A	0.8	N/A
Particle density [kg·m^{-3}]	2100	2500	2600	3066
Particle diameter [μm]	200	209	270	299
Suspension density [kg·m^{-3}]	2–40	9.2	15–70	60
Riser diameter [m]	3.96 × 3.96 × 23	5.13 × 5.13 × 28	1.4 × 1.7 × 13.5	0.15 × 0.15 × 7.3
Gas velocity [m·s^{-1}]	6.4	N/A	4–6	6.5–8.6
h_r (estimated by authors) [W·m^{-2}·K^{-1}]	100	109	75–80	68
h_r/h [W·m^{-2}·K^{-1}]	50%	33% and 63%	46–67%	64%
Predicted h_r by the Model [W·m^{-2}·K^{-1}]	91	96	79–90	56

N/A = Not Available.

Table 3
Operating conditions and comparison of model prediction with the experimental h_r data

Author	Luan et al. [42]	Basu and Konuche [48]	Han and Cho [49]
Bulk temperature [°C]	800–900	650, 885	650–850
Probe surface or wall temperature [°C]	25–189	50, 70	N/A
Probe surface or wall emissivity	0.9	N/A	0.7
Particle density [kg·m^{-3}]	2610	2650	2600[a]
Particle diameter [μm]	286 & 334	296	450
Suspension density [kg·m^{-3}]	20–90	4–30	20–30
Riser diameter [m]	015 × 015 × 7.3	0.2 × 0.2 × 6.7	0.2 × 0.2 × 6.0
Gas velocity [m·s^{-1}]	8	8–11	3.0–5.0
Measured h_r [W·m^{-2}·K^{-1}]	19–143	45, 110	60–120
Predicted h_r by the model [W·m^{-2}·K^{-1}]	11–98	47, 86	for $T_w = 100$ °C 44–83 for $T_w = 250$ °C 57–96

N/A = Not Available.
[a] Estimated value.

out on sand particles of mean size 296 μm, at local suspension densities 4–30 kg·m^{-3}, and over a bed temperature range 500–900 °C. Basu and Konuche [48] reported that the radiative component is 74–91% of the total heat flux transferred from suspension to the wall. This is much higher than other reported values in the literature for the direct radiative heat transfer measurements that are between 15–36% [49]; 22–38% [42], and for indirect, 50% [7]; 46–67% [31]; and 25–50% [36]. Fig. 3 compares the model predictions and experimental results. The model substantially underestimates radiative heat transfer coefficients at higher temperatures, while the predictions are quite close at lower temperatures. One reason for the deviations could be that heat conducted through the windows could not be removed totally. Another reason could be that the body of the probe was assumed to be insulated such that conduction took place in one dimension only; failing this make that higher heat flux was recorded and it will increase with suspension temperature. Another possible cause is that the model does not consider the dependency of e_b on the bed temperature as reported by Baskakov [50].

Luan et al. [42] reported experimental local radiative heat transfer coefficients at temperatures from 200 to 900 °C and at local cross-sectional average suspension densities from 20 to 90 kg·m^{-3}. The riser was 152 mm square in cross section and 7.3 m high. The radiative heat fluxes were estimated using both the differential emissivity method and the window method for sand of mean diameters 286 and 334 μm. The surface temperature varied between 25 and 189 °C [51]. Fig. 4 shows the experimental and predicted local radiative heat transfer coefficients as a function of suspension temperature. Data from Luan et al. [42] exceeds simulation results

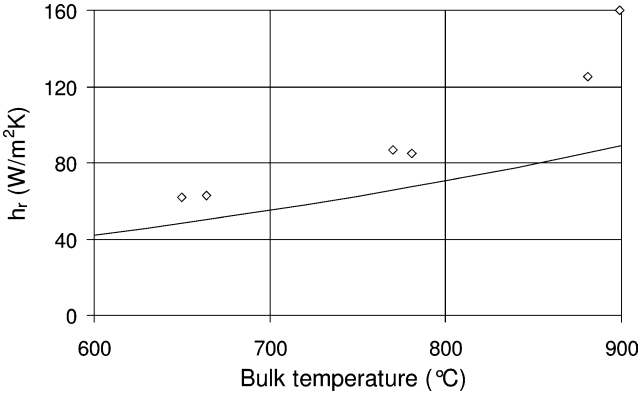

Fig. 3. Comparison of predicted radiative heat transfer coefficient with experimental data of Basu and Konuche [48] for different suspension temperature. Operating conditions are listed in Tables 1 and 3. $d_p = 296$ μm; $\rho_{sus} = 4$–30 kg·m^{-3}; $\rho_p = 2650$ kg·m^{-3}. Line shows predicted results.

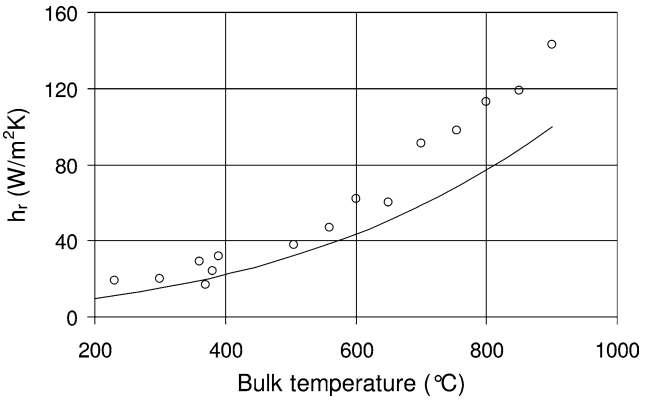

Fig. 4. Comparison of predicted radiative heat transfer coefficient with experimental data of Luan et al. [42] for different suspension temperature. Operating conditions are listed in Tables 1 and 3. $d_p = 286$ μm; $\rho_{sus} = 50$ kg·m^{-3}; $\rho_p = 2610$ kg·m^{-3}. Line shows predicted results.

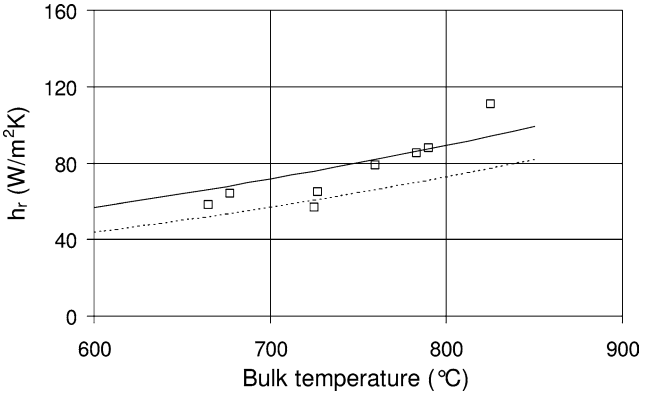

Fig. 5. Comparison of predicted radiative heat transfer coefficient with experimental data of Han and Cho [49] for different suspension temperature. Operating conditions are listed in Tables 1 and 3. $d_p = 450$ μm; $\rho_{sus} = 20$–30 kg·m^{-3}; $\rho_p = 2600$ kg·m^{-3}. Lines show predicted results: solid ($T = 250\,^{\circ}$C) and dashed ($T = 100\,^{\circ}$C).

from the model at higher temperatures. One possible explanation for this could be that they did not fully succeed in isolating the radiation component, and has received a contribution from convection/conduction at higher temperatures. This would be reinforced by combustion gas conductivity, which increases with temperature. A second explanation could be that the suspension and/or riser emissivities may have been larger at higher temperatures.

In Fig. 5 the experimental data of Han and Cho [49] at superficial gas velocity of 4 m·s^{-1}, suspension density of 25 kg·m^{-3}, particle diameter of 450 μm in a CFB riser with 0.2×0.2 m in cross-section are compared with model predictions at wall temperatures of 100 and 250 °C, since the actual wall temperatures were not available. The radiation probe consisted of a brass body, calcium fluoride window and heat flux transducer. The diameter of the sensor is 6.35 mm and it is water-cooled. In the calculations $e_p = 0.6$ and $e_w = 0.8$ were used. At highest temperature, the figure shows the same tendency as discussed in the comparisons to Luan et al. [42] and Basu and Konuche [48] above. Because

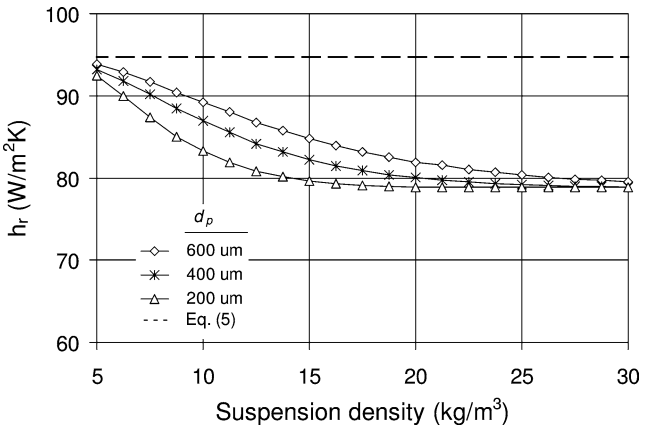

Fig. 6. Influence of suspension density and particle diameter on radiative heat transfer coefficient.

of the unknown wall temperature we will not draw other conclusions.

3.2. Sensitivity analysis

The model is used to study influence of various parameters on the radiative heat transfer coefficient in CFB combustors. The most important parameters such as suspension temperature, wall temperature, particle emissivity, wall emissivity, suspension density, particle diameter, and the riser diameter are studied. The base case operating conditions are shown in Table 1.

If suspension density is set to $\rho_{sus} = 0$ in the model, no attenuation of radiative heat transfer from particles in the suspension occurs, and the same results should be achieved as by using Eq. (5) with the same emissivity values. Then particles are introduced with increasing of suspension density levels in the model and h_r gradually decreases below the prediction of Eq. (5). Fig. 6 shows that the radiative heat transfer coefficient decreases with suspension density as expected. This is due to increase in several related factors such as particle concentration of the clusters, fraction of wall covered by clusters, and wall layer thickness. This shows that decreasing suspension density decreases the total heat transfer coefficient while h_r increases. This is more significant in commercial CFB boilers where the suspension density varies between 2 to 17 kg·m^{-3} [52]. This figure shows also that the h_r increases with increasing particle diameter. This is due to the decreased attenuation of the emitted and scattered radiation from different optical depths in the clusters as well as in the dispersed/dilute phase, as reported by Brewster [39]. The dashed line in this figure indicates the maximum radiative heat transfer coefficient, Eq. (5).

The radiative heat transfer coefficient increases as suspension temperature increases (Fig. 7). This is consistent with the experimental results reported by, e.g., Basu and Konuche [48], Luan et al. [42] and Han and Cho [49]. h_r increases also with increasing wall temperature as shown in this figure.

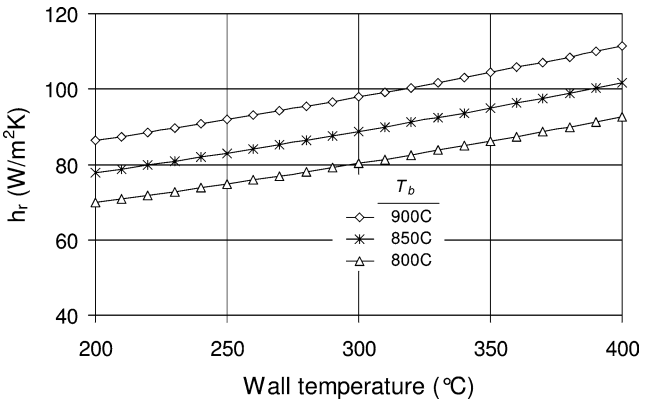

Fig. 7. Radiative heat transfer coefficient as a function of wall temperature and suspension temperature.

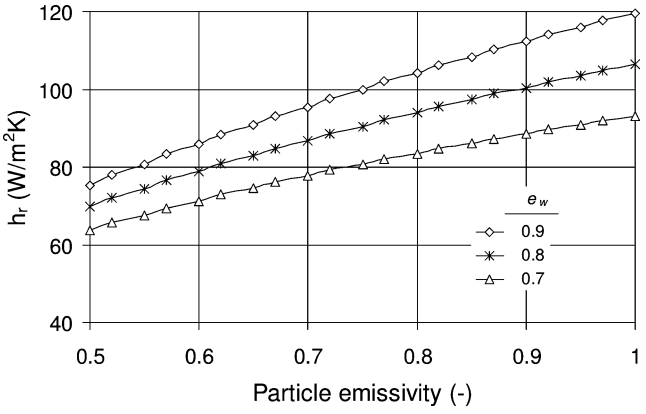

Fig. 8. Radiative heat transfer coefficient as a function of particle emissivity and wall emissivity.

The particle emissivity value used in this study ($e_p = 0.6$) is uncertain. One reason for this is that from the first day of use the sand particles are coated by mainly a mixture of Ca- and Mg-silicates as well as P and are mixed with ashes especially when biomass fuels are used, Brus et al. [53] and Sjösten et al. [54]. Values of $0.6 \leqslant e_p \leqslant 0.85$ and $0.7 \leqslant e_w \leqslant 1.0$ are used in the literature see, e.g., [31,42, 55]. The influence of particle and wall emissivities is illustrated in Fig. 8. This figure indicates that h_r increases with increasing either particle emissivity or wall emissivity. It is obvious that assuming a certain particle or wall emissivity will greatly affect the predicted results. For example varying e_p from 0.6 to 0.85, at $e_w = 0.8$ leads to 23% increase of the radiative heat transfer coefficient. This increases even more at higher wall emissivities.

Fig. 9 shows that above a suspension density of 2 kg·m^{-3}, increasing riser diameter leads to decreasing h_r. This can be explained by decreasing wall area in comparison to riser volume, which causes a thicker wall layer and thus a stronger radiation shield. Curves representing 5 and 10 kg·m^{-3} in suspension densities, show how the wall layer builds up and decreases the h_r. This effect has almost vanished at a suspension density of 20 kg·m^{-3}, and at 30 kg·m^{-3} riser diameters show no significant influence on radiative heat transfer coefficient. This suggests that at this suspension density, the wall layer is already fully developed at a riser diameter of 2 m.

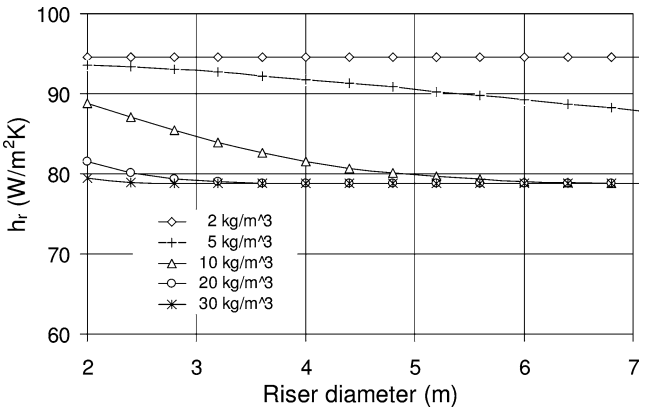

Fig. 9. Influence of riser diameter and suspension density on radiative heat transfer coefficient.

4. Conclusions

A new model, based on the two flux method, is proposed to determine local radiative heat transfer coefficients on walls of the furnace of a circulating fluidized bed combustor. The model contains several parameters and the difficulties in estimating these were thoroughly discussed. It was found that the model predictions were in good agreement with experiments at lower temperatures and underestimates at higher temperatures. The deviation may be due to the experimental results having a contribution from convection/conduction especially at higher temperatures.

The simulation results indicate that radiation heat transfer coefficients increase with bulk temperature, wall temperature, wall emissivity and particle emissivity. But radiation heat transfer coefficients decrease significantly with suspension density at suspension densities less than 20 kg·m^{-3}. Influences of particle size and riser diameter on the h_r are limited to lower suspension densities in CFB's of industrial size.

Acknowledgements

The discussions with and the comments of Professor J.R. Grace are greatly appreciated.

References

[1] R.L. Wu, C.J. Lim, J. Chaouki, J.R. Grace, Heat transfer from a circulating fluidized bed to membrane waterwall surfaces, AIChE J. 33 (1987) 1888–1893.

[2] B. Leckner, M.R. Golriz, W. Zhang, B.-Å. Andersson, F. Johnsson, Boundary layers—first measurements in the 12 MW CFB research plant at Chalmers University of Technology, in: E.J. Anthony (Ed.), Proc. 11th Int. Conf. on Fluidized Bed Combustion, vol. 2, 1991, pp. 771–776.

[3] R.C. Senior, C. Brereton, Modeling of circulating fluidized bed solids flow and distribution, Chem. Engrg. Sci. 47 (1992) 281–296.
[4] P. Basu, Heat transfer in high temperature fast fluidized beds, Chem. Engrg. Sci. 45 (1990) 3123–3136.
[5] J.R. Grace, Heat transfer in high velocity fluidized beds, in: G. Hetsroni (Ed.), Proc. 9th International Heat Transfer Conference, vol. 1, Jerusalem, 1990, pp. 329–339.
[6] J.R. Grace, Influence of riser geometry on particle and fluid dynamics in circulating fluidized beds risers, in: L.M. Kwauk, J. Li (Eds.), Circulating Fluidized Bed Technology V, Science Press, Beijing, 1996, pp. 16–26.
[7] F.R. Steward, M.F. Couturier, S. Poolpol, Analysis for radiative heat transfer in a circulating fluidized bed, in: K.J. Heinschel (Ed.), Proc. 13th Int. Fluidized Bed Combustion Conference, vol. 1, ASME, New York, 1995, pp. 507–513.
[8] W. Zhang, Fluid dynamics of the transport zone of circulating fluidized beds—with application to boilers, Ph.D. Thesis, Chalmers University of Technology, Gothenburg, Sweden, 1995.
[9] M.R. Golriz, Influence of wall geometry on local temperature distribution and heat transfer in circulating fluidized bed boilers, in: A. Avidan (Ed.), Circulating Fluidized Bed Technology IV, AIChE, New York, 1994, pp. 693–700.
[10] C.C. Werdermann, J. Werther, Heat transfer in large-scale circulating fluidized bed combustors of different sizes, in: A.A. Avidan (Ed.), Circulating Fluidized Bed Technology IV, AIChE, New York, 1994, pp. 428–435.
[11] M.R. Golriz, J.R. Grace, Predicting heat transfer in large-scale CFB boilers, in: J.R. Grace, J. Zhu, H. de Lasa (Eds.), Circulating Fluidized Beds Technology VII, Canadian Society for Chemical Engineering, Ottawa, 2002, pp. 121–128.
[12] M.Q. Brewster, C.L. Tien, Examination of the two-flux model for radiative transfer in particulate systems, Internat. J. Heat Mass Transfer 25 (1982) 1905–1907.
[13] H. Kobro, C. Brereton, Control and fuel flexibility of circulating fluidized beds, in: P. Basu (Ed.), Circulating Fluidized Bed Technology, Pergamon, Toronto, 1986, pp. 263–272.
[14] D. Subbarao, P. Basu, A model for heat transfer in circulating fluidized beds, Internat. J. Heat Mass Transfer 29 (1986) 487–489.
[15] J.C.L. Furchi, L. Goldstein Jr, G. Lombardi, M. Mohseni, Experimental local heat transfer in a circulating fluidized bed, in: P. Basu, J.F. Large (Eds.), Circulating Fluidized Bed Technology II, Pergamon, Toronto, 1988, pp. 263–270.
[16] B.-A. Andersson, B. Leckner, Experimental methods of estimating heat transfer in circulating fluidized bed boilers, Internat. J. Heat and Mass Transfer 35 (1992) 3353–3362.
[17] M.R. Golriz, B. Sunden, An experimental investigation of thermal characteristics in a 12 MWth CFB boiler, Experimental Heat Transfer J. 7 (1994) 217–233.
[18] P. Basu, P.K. Nag, Heat transfer to walls of a circulating fluidized-bed furnace, Chem. Engrg. Sci. 51 (1996) 1–26.
[19] B.-A. Andersson, Effect of bed particle size on heat transfer in circulating fluidized bed boilers, Powder Technol. 87 (1996) 239–248.
[20] A. Dutta, P. Basu, in: Int. Fluid Bed Combustion Conf. Jacksonville, Florida, 2003.
[21] X.T. Bi, J. Zhou, S.Z. Qin, J.R. Grace, Annular wall layer thickness in circulating fluidized bed risers, Canad. J. Chem. Engrg. 74 (1996) 811–814.
[22] P.D. Noymer, M.R. Hyre, L.R. Glicksman, The influence of bed diameter on hydrodynamics and heat transfer in circulating fluidized beds, in: Fluidization and Fluid Particle Systems, AIChE, New York, 1995, pp. 86–90.
[23] J. Werther, Fluid mechanics of large-scale CFB units, in: A.A. Avidan (Ed.), Circulating Fluidized Bed Technology IV, AIChE, New York, 1994, pp. 1–14.
[24] R. Bader, J. Findlay, T.M. Knowlton, Gas/solid flow patterns in a 30.5-cm-diameter circulating fluidized bed, in: P. Basu, J.F. Large (Eds.), Circulating Fluidized Bed Technology II, Pergamon, Toronto, 1988, pp. 123–137.
[25] M. Lints, L.R. Glicksman, Parameters governing particle-to-wall heat transfer in a circulating fluidized bed, in: A. Avidan (Ed.), Circulating Fluidized Bed Technology IV, AIChE, New York, 1994, pp. 297–304.
[26] L.R. Glicksman, Heat transfer in circulating fluidized beds, in: J.R. Grace, A.A. Avidan, T.M. Knowlton (Eds.), Circulating Fluidized Beds, Chapman and Hall, London, 1997, pp. 261–311, Chapter 8.
[27] J.C. Chen, J.R. Grace, M.R. Golriz, Heat transfer in fluidized beds, design methods, Powder Technol. (2004), in press.
[28] R.L. Wu, C.J. Lim, J.R. Grace, C.M.H. Brereton, Instantaneous local heat transfer and hydrodynamics in a circulating fluidized bed, Internat. J. Heat Mass Transfer 34 (1990) 2019–2027.
[29] M.R. Golriz, J.R. Grace, Augmentation of heat transfer by deflectors on circulating fluidized bed membrane walls, Internat. J. Heat Mass Transfer 45 (2002) 1149–1154.
[30] K.E. Wirth, M. Seiter, Solids concentration and solids velocity in the wall region of circulating fluidized beds, in: E.J. Anthony (Ed.), Proc. 11th Int. Conf. on Fluidized Bed Combustion, vol. 1, 1991, pp. 311–315.
[31] M.R. Golriz, B. Sunden, An analytical-empirical model to predict heat transfer coefficients in circulating fluidized bed combustors, Wärme und Stoff Ubertragung 30 (1995) 377–383.
[32] M.R. Golriz, An experimental correlation for temperature distribution at the membrane wall of CFB boilers, in: K.J. Heinschel (Ed.), Proc. 13th Int. Fluidized Bed Combustion Conference, vol. 1, ASME, New York, 1995, pp. 499–505.
[33] D. Xie, Modeling of heat transfer in circulating fluidized beds, Ph.D. Thesis, University of British Columbia, Vancouver, Canada, 2001.
[34] M.R. Golriz, Heat transfer determination in CFB boiler water-wall tubes using a heat flux meter, in: Proc. Swedish-Finnish Flame Days 1993, Gothenburg, 1993, pp. 222–226.
[35] R.L. Wu, J.R. Grace, C.J. Lim, C. Brereton, Suspension-to-surface heat transfer in a circulating fluidized bed combustor, AIChE J. 35 (1989) 1685–1691.
[36] G. Flamant, B. Variot, M.R. Golriz, J.D. Lu, Radiative heat transfer in a pilot scale circulating fluidized bed boiler, in: L.M. Kwauk, J. Li (Eds.), Circulating Fluidized Bed Technology V, Science Press, Beijing, 1996, pp. 563–568.
[37] R. Siegel, J.R. Howell, Thermal Radiation Heat Transfer, third ed., Hemisphere, Washington, DC, 1992.
[38] M.N. Ozisik, Radiative Transfer and Interactions with Conduction and Convection, Wiley, New York, 1973.
[39] M.Q. Brewster, Effective absorptivity and emissivity of particulate media with application to fluidized bed, Trans. ASME J. Heat Transfer 108 (1986) 710–713.
[40] J.C. Chen, R.J. Cimini, S. Dou, A theoretical model for simultaneous convective and radiative heat transfer, in: P. Basu, J.F. Large (Eds.), Circulating Fluidized Bed Technology II, Pergamon, Toronto, 1988, pp. 255–262.
[41] M. Eriksson, Radiation heat transfer in circulating fluidized bed combustors, MSc. Thesis, Umea University, 2002.
[42] W. Luan, C.J. Lim, C.M.H. Brereton, B.D. Bowen, J.R. Grace, Experimental and theoretical study of total and radiative heat transfer in circulating fluidized beds, Chem. Engrg. Sci. 54 (1999) 3749–3764.
[43] A.S. Issangya, J.R. Grace, D. Bai, J. Zhu, Radial voidage variation in CFB risers, Canad. J. Chem. Engrg. 79 (2001) 279–286.
[44] H.M. Shafey, I.S. Taha, A.S. Huzayyin, Computer-aided simulation of fluidized bed combustor, in: Proceedings of the ASME 1989, Winter Annual Meeting, in: Analysis and Design of Energy Systems: Computer-Aided Engineering, vol. 10-1, ASME United Engineering Center, New York, 1989, pp. 43–52.
[45] M. Lints, Particle-to-wall heat transfer in circulating fluidized beds, Doctoral Thesis, Massachusetts Institute of Technology, 1992.
[46] Nucla Circulating Atmospheric Fluidized Bed Demonstration Project, Final Report, DOE/MC/25137-3046, 1991.
[47] M.F. Couturier, F.R. Steward, S. Poolpol, Experimental determination of heat transfer coefficients in a 72 MWth circulating fluidized bed boiler, in: L.N. Rubow (Ed.), Proc. 12th Int. Conf. on Fluidized Bed Combustion, 1993, pp. 1215–1222.

[48] P. Basu, F. Konuche, Radiative heat transfer from a fast fluidized bed, in: P. Basu, J.F. Large (Eds.), Circulating Fluidized Bed Technology II, Pergamon, Toronto, 1988, pp. 245–253.
[49] G.Y. Han, Y.J. Cho, Radiative heat transfer in a circulating fluidized bed coal combustor, in: Powder Technology, vol. 102, Elsevier, Amsterdam, 1998, pp. 266–273.
[50] A.P. Baskakov, Heat transfer in fluidized beds: Radiative heat transfer in fluidized beds, in: J.F. Davidson, R. Clift, D. Harrison (Eds.), Fluidization, Academic Press, London, 1985.
[51] W. Luan, Radiative and total heat transfer in circulating fluidized beds, Ph.D. Thesis, University of British Columbia, Vancouver, Canada, 1997.
[52] M.R. Golriz, Temperature distribution at the membrane wall of a 165 MWth CFB boiler, Experimental Heat Transfer J. 14 (2001) 299–313.
[53] E. Brus, M. Öhman, A. Nordin, B.-J. Skrifvars, R. Backman, Bed material consumption in biomass fired fluidised bedboilers due to risk of bed agglomeration—coating formation and possibilities for regeneration, IFRF Combust. J. 200302 (2003).
[54] J. Sjösten, M.R. Golriz, A. Nordin, J.R. Grace, Effects of particle coating on fluidized bed heat transfer, Indust. Engrg. Chem. Res. 43 (2004) 5763–5769.
[55] D. Xie, B.D. Bowen, J.R. Grace, C.J. Lim, Two-dimensional model of heat transfer in circulating fluidized beds. Part I: Model development and validation, Internat. J. Heat Mass Transfer 46 (2003) 2179–2191.